Experiments on whistler mode electron-cyclotron resonance plasma startup and heating in an axisymmetric magnetic mirror

J. H. Booske,[a] W. D. Getty,[b] and R. M. Gilgenbach[a]
College of Engineering, University of Michigan, Ann Arbor, Michigan 48109

R. A. Jong
Lawrence Livermore National Laboratory, Livermore, California 94550

(Received 11 February 1985; accepted 23 June 1985)

Whistler mode electron-cyclotron resonance heating (ECRH) has been performed simultaneously with whistler mode electron-cyclotron emission measurements on an axisymmetric magnetic mirror plasma. Results presented include a study of the early plasma startup phase and two instability phases, one believed to be caused by a whistler instability and another by magnetohydrodynamic (MHD) flute instability. Enhanced microwave emission at frequencies below the midplane electron-cyclotron frequency has been correlated with enhanced electron endloss during the whistler instability. Cyclotron emission spectra during the startup phase match predictions for a "sloshing electron" type distribution based on numerical modeling. This distribution also agrees with anisotropic distributions resulting from electron-cyclotron heating as predicted by Fokker–Planck computer simulations. Experimentally measured heating rates show good agreement with simplified analytical models based on stochastic heating.

I. INTRODUCTION

The eventual goal of a viable magnetic mirror fusion reactor will require mastery of numerous technological challenges. Significant progress, however, was achieved with the demonstration that technological constraints on plasma heating could be eased by supplementing or replacing neutral beam power with rf power.[1] Recent research, recognizing the need for improved confinement, has emphasized the development of "thermal barriers" to isolate end-plug and central-cell electrons in tandem mirrors.[2,3] The advantages of using electron-cyclotron resonance heating (ECRH) for producing thermal barriers, as well as plasma startup and subsequent heating in magnetic mirror devices, have been well established.[4,5] In most instances, however, the ECRH microwave power has been launched perpendicularly to the magnetic axis of symmetry.[4,6,7] The goal of the experiments reported here was to investigate the effects of an alternative in which the microwave energy is launched at small angles relative to the magnetic axis, i.e., the whistler mode. Possible advantages of the whistler mode include the absence of a density cutoff[5] (when the wave frequency f_s is less than the local electron-cyclotron frequency f_{ce}), and the potential for off-axis profiling of electron density and temperature (which has applications for ring-stabilized axisymmetric systems, as well as mantle electron generation for octopole-stabilized mirrors).[8]

In this article we present experimental results on ECRH startup and subsequent heating using the whistler mode in an axisymmetric mirror, including time-resolved whistler electron-cyclotron emission (WECE) spectra, endlosses, heating rate estimates, and the characterization of both a microinstability and a macroinstability.

II. EXPERIMENTAL CONFIGURATION AND OPERATION

A. Description of magnetic-mirror apparatus

The experiment is performed on a small axisymmetric magnetic mirror device operated in a repetitively pulsed mode (1 pulse/1.5 sec). The general layout of the central region of the apparatus is shown in Fig. 1. The vacuum vessel in the midplane region is a 10 cm diam metal tube. It is terminated on one end by a 45 cm diam end tank and on the other end by a 10 cm four-way cross. The transmitting horn antenna is located in the end tank and the receiving horn antenna is located in the cross. Both are outside of the mirror peaks. Two oil diffusion pumps and a turbomolecular pump are used for vacuum pumping. A base pressure in the range of $5–7\times10^{-7}$ Torr has been obtained.

The mirror ratio is 2-to-1 and the midplane magnetic field at the "standard" operating conditions of the experiment is 2.34 kG, corresponding to a midplane electron-cyclotron frequency of 6.55 GHz. The distance between mirror peaks is 49 cm. Magnets are run with direct current.

Microwave power is launched from a novel, dielectric-loaded, horn antenna located inside the vacuum system in a position at the junction between the end tank and the 10 cm tube. By inserting a tapered, rectangular, Teflon rod into the end of a short, small-aperture horn antenna, it was possible to improve the wave-launching conditions from a 30° (− 3 dB point), half-angle, standard 10-dB-gain horn antenna to a 9°, half-angle, 20-dB-gain launching structure. The transmission horn antenna axis is aligned approximately with that of the tube.

The microwave heating pulse has a maximum duration of 400 μsec and a peak power of up to 1000 W at 7.43 GHz. To generate this power, the output of a low power (50 mW), cw reflex klystron oscillator is fed to a Varian 856*B* four-cavity klystron amplifier. The pulsed high-power microwave signal is then generated by applying a negative high-voltage pulse to the amplifier cathode. By varying the

[a] Department of Nuclear Engineering.
[b] Department of Electrical Engineering and Computer Science.

 0031-9171/85/103116-11$01.90

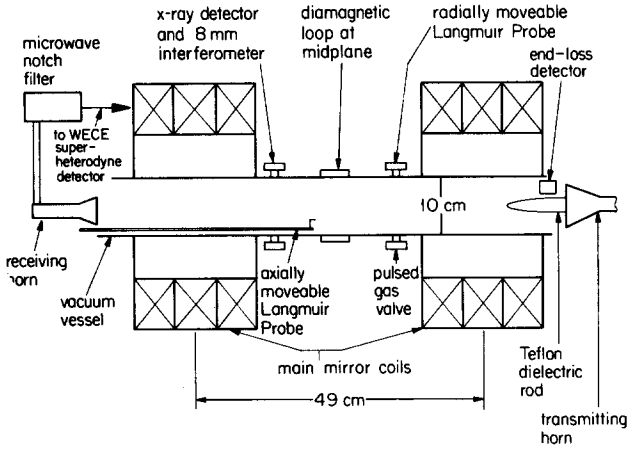

FIG. 1. Michigan mirror machine (MIMI).

voltage pulse level, one can vary the power launched to the plasma. Very rapid modulations (less than 15 μsec) of the high-power microwave signal are also possible by slight voltage modulations on the reflector grid of the oscillator, thus momentarily detuning the oscillator and the amplifier. The microwave pulse repetition period is determined by the pulsed gas valve and is 1.5 sec. The receiving horn antenna is also coaxial with the vacuum tube.

Figure 1 shows the location of the pulsed gas valve used to inject the working gas (hydrogen) into the midplane region. Gas puffing produces a transient pressure pulse in the midplane region that contains an initial peak of 200–300 μsec duration followed by a millisecond time-scale pumpout to base pressure before the next pulse. On the time scale of the plasma pulse, the gas pressure is essentially constant at the time the microwave pulse is injected, although plasma pumpout effects are probably important. Steady gas flow can also be provided by a needle valve. A fast ionization gauge is used to measure gas transients in the midplane region.

The diagnostics used in the work reported here are also shown in Fig. 1. The primary diagnostics used in our experiments were diamagnetic loops, electrostatic probes, a net endloss detector (NELD), time-resolved WECE spectra, a foil-filtered scintillation x-ray detector, and an 8 mm microwave interferometer.

The NELD consists of a single grounded entrance grid with an approximately 1 cm diameter transmission aperture. Immediately behind the grid is a voltage-biased collecting electrode. This assembly is located outside the mirror magnetic peaks at an axial location where the magnetic flux density is approximately equal to that at the mirror midplane. In addition, the NELD samples electron endloss along a magnetic flux line that maps to a radius of approximately 2.5 cm at the mirror midplane.

The x-ray detector uses a fast-response plastic scintillator (NE-102) that is shielded from plasma electrons and optical emission by a 7 μm thick aluminum foil filter. The filtered scintillator tip is positioned inside the vacuum vessel in order to view the mirror-trapped plasma along the magnetic axis. Scintillation photons are transmitted by a foil-covered lucite light guide to a magnetically shielded photomultiplier tube (PMT) located outside the vacuum vessel. The signal from the PMT is then recorded on an oscilloscope using a 50 Ω input impedance.

It has been recently demonstrated that WECE is a valuable diagnostic for mirror plasmas.[9,10] In principle, one can obtain information on the axial variation of plasma electron temperature and density. We have found that the WECE spectrum, observed in a time-resolved manner, is an especially valuable diagnostic for studying ECRH startup and other time variant phenomena. The relative spectra have provided information on plasma axial extent, electron velocity distribution anisotropy, upper bounds for electron temperatures, and the presence of "cold" and "hot" electron population components, as well as the axial location(s) where a microinstability originates. The WECE radiometer is a superheterodyne circuit consisting of a broadband (2–18 GHz) local oscillator, a broadband, low-loss, microwave mixer (4–18 GHz), a 0.1–1500 MHz spectrum analyzer, and a custom-fabricated, stripline microwave notch filter that provides more than 50 dB attenuation between 7.4 and 7.5 GHz (i.e., the heating frequency), but less than 2 dB attenuation for other frequencies in the 4–15 GHz range.

B. Operation of apparatus

The experiment is operated at a microwave pulse repetition period of 1.5 sec and steady magnetic field. At this rate the operator can make numerous, nearly continuous adjustments of plasma and diagnostic operating conditions before taking data on a series of consecutive pulses. The plasma is moderately reproducible from discharge-to-discharge under typical operating conditions and very reproducible under certain conditions. The plasma buildup is very sensitive to the amount of injected gas and to the background steady-state gas pressure. There can be long term (approximately 1 hour) variations in the plasma behavior that are apparently caused by slow changes in absorbed gas on the walls. In general, plasma reproducibility is satisfactory for experimental runs of several hours. With pulsed gas operation the microwave pulse is timed to be fired immediately after the initial transient pressure peak in the midplane region. This is approximately 300 μsec after gas initially appears at the midplane. It was found that the plasma was less reproducible if the pulse was fired earlier when the pressure was changing rapidly. The plasma diamagnetism is used as a guide in adjusting the gas so that peak diamagnetism occurs 200 to 300 μsec after the start of the microwave pulse. The peak diamagnetism occurs earlier when the gas feed is increased but its magnitude also decreases significantly. Under optimum conditions the midplane pressure is estimated to be $3-6\times10^{-5}$ Torr at the time of the microwave pulse.

The system can be operated with pulsed or steady gas injection or a combination of both. Steady flow with either hydrogen or nitrogen is used to simulate the effect of higher base pressure. It is found that plasma buildup and stability are affected by increased background pressure. This effect is discussed in more detail below.

Time-resolved WECE measurements are obtained by sending the receiving horn signal through the notch filter (to protect the sensitive detection equipment from the high-power ECRH signal), to be mixed with the local oscillator

signal. This IF signal is then fed to the spectrum analyzer (run in fixed frequency mode at 20 MHz IF with a 3 MHz resolution bandwidth). The spectrum analyzer provides a calibrated video signal output which is fed to an oscilloscope with differential amplifier for time resolved measurements. WECE spectra are obtained by performing a rapid series of discharges in which the local oscillator frequency (and thus the detected emission frequency) is varied between discharges. At the end of a run, those discharges for which plasma conditions were identical (as indicated by the other diagnostic signals) are selected to determine spectra.

To establish that the rf/plasma interaction was dominated by single-pass whistler wave absorption rather than by microwave cavity modes, a microwave absorbing target was inserted near the vacuum vessel end wall, in place of the WECE receiving horn. The target made use of a commercial material (Emerson and Cuming, Eccosorb SF-7.5) that was designed for -25 dB of attenuation at normal incidence of 7.5 GHz microwaves. The effectiveness of this target for eliminating microwave end-wall reflections was confirmed by independent test measurements in an identical section of vacuum tubing. Replacement of the WECE receiving horn by this microwave "beam dump" led to no observable changes in the measured plasma properties. In addition to these tests it was found under normal operating conditions that nearly all of the incident ECRH microwaves were absorbed by the plasma during the startup phase. Finally, peak electron densities (2.3×10^{12} cm^{-3}), as measured by the interferometer, exceeded the critical density for the 7.43 GHz heating frequency (6.8×10^{11} cm^{-3}). Nevertheless, reflected microwave power did not increase at high density. The above-mentioned observations provided convincing evidence that the rf heating was dominated by strong, single-pass, whistler wave absorption and that microwave cavity and/or waveguide modes were not responsible for the observed plasma behavior.

It was also important to demonstrate that the measured cyclotron emissions were truly representative of whistler emissions, which propagate at small angles to the magnetic field, and did not include some component of perpendicular emissions caused by vessel wall reflections. This was accomplished by replacing the simple horn antenna used for WECE detection by a narrow-gain-pattern, dielectric-loaded horn antenna, similar to the ECRH launching antenna. The resulting relative emission spectra were identical to those detected by the previous horn antenna, with the exception of a decrease in signal amplitude. This reduction of absolute signal strength roughly correlated to that expected for the decreased detection solid angle because of the narrowed antenna gain pattern. In addition, previous investigators[11] have also found that with the introduction of microwave absorbing liners, only the emission measured perpendicular to the magnetic axis was altered, whereas whistler emission measured at small angles to the magnetic field remained essentially unchanged.

III. EXPERIMENTAL RESULTS AND DISCUSSION

Data from a typical discharge are presented in Figs. 2 and 3. To assist in establishing temporal correlations, the 6.5 GHz WECE signal of Fig. 2(b) has been repeated as Fig. 3(f). Based on these diagnostic signals we have found it convenient to divide discussion of the evolution of this plasma into three temporal regimes. Regime A includes ECRH startup and heating, apparently free from instabilities. Regime B involves a microinstability that we have tentatively identified as a whistler instability. It is characterized by a strong burst of microwave emission at frequencies slightly below the midplane fundamental electron-cyclotron frequency, enhanced endlosses caused by electrons leaving the midplane region, and rapid transition of midplane potential from small, negative values (0 to − 15 V) to large, positive values (70 to 100

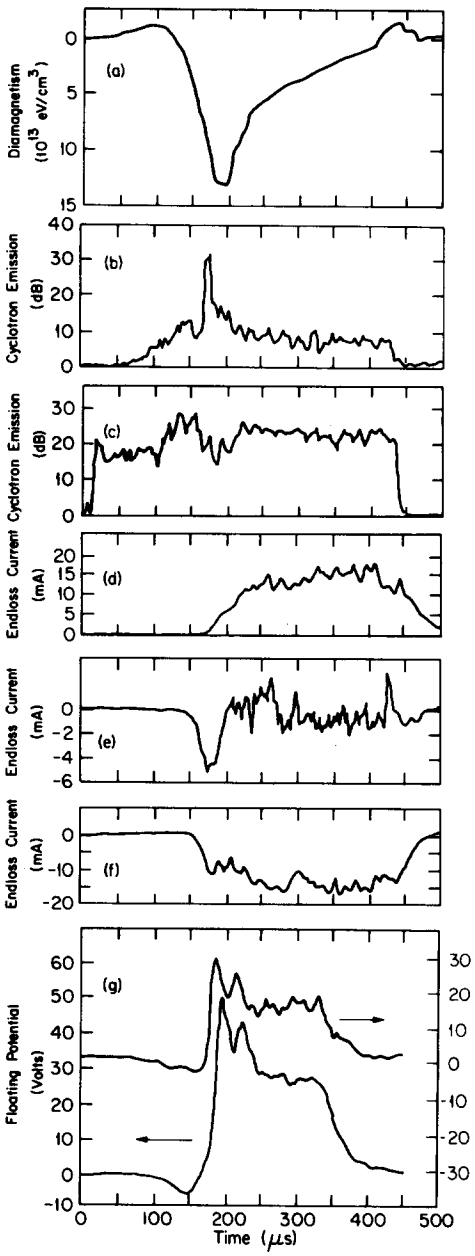

FIG. 2. Typical diagnostic data: (a) integrated diamagnetic loop; (b) 6.5 GHz WECE power; (c) 7.6 GHz WECE power; (d) net endloss current, collector biased at − 30 V; (e) net endloss current, collector biased at 5 V; (f) net endloss current, collector biased at 30 V; (g) floating potential for two probes located at 90° apart, azimuthally. Upper trace from axially fixed (radially moveable) probe at $z = 7$ cm, $r = 1.75$ cm, lower trace from axially moveable (radially fixed) probe at $z = 6$ cm, $r = 1.75$ cm.

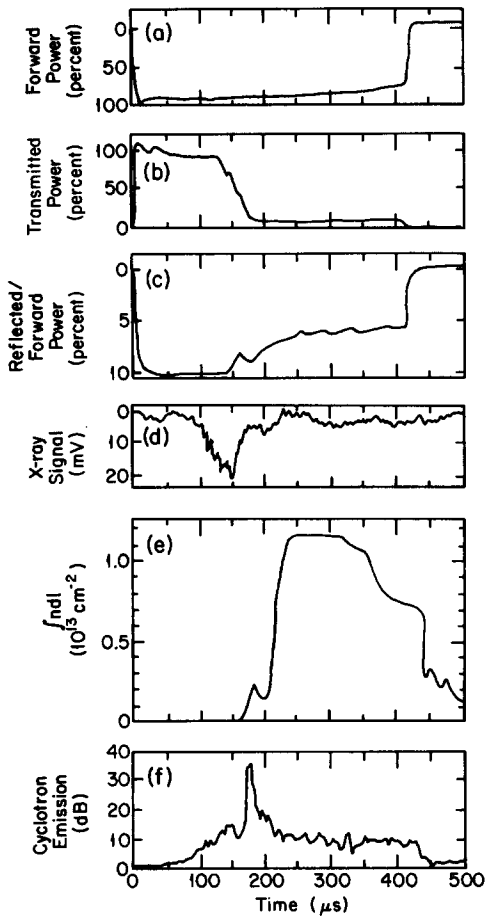

FIG. 3. Typical diagnostic data: (a) forward ECRH power; (b) ECRH power transmitted through the plasma; (c) reflected ECRH power as a percentage of forward power; (d) x-ray signal into 50 Ω; (e) radially averaged electron density from interferometer; (f) 6.5 GHz WECE signal repeated for temporal correlations.

V). Regime C is dominated by a MHD instability and is characterized by significant endlosses (predominantly ions), steady cyclotron emissions, axial plasma expansion, positive plasma potentials, and fluctuations on many signals in the 20 to 100 kHz range. We will now discuss the experimental results during each regime in more detail.

A. Regime A

As previously mentioned, this regime characterizes the early phases of ECRH startup and subsequent heating, apparently free from instabilities. Initially (0 to 50 μsec), there is evidence of rapid creation of a low density plasma. This initial plasma has sufficient energy to generate detectable levels of fundamental WECE signals [Fig. 2(c)], but lacks sufficient density or energy to register diamagnetism [Fig. 2(a)], Doppler-shifted WECE [Fig. 2(b)], or x-ray signals [Fig. 3(d)]. Furthermore, little microwave absorption occurs during this very early phase [Figs. 3(b) and 3(c)]. Shortly afterward, however, (between 50 and 100 μsec) this low density plasma experiences an increase in temperature because of the rf heating. This is demonstrated by the appearance of both Doppler-shifted WECE and x-ray signals. Electron densities at this time, however, are still too low to provide any detectable diamagnetism. By 100 μsec we observe an almost exponential increase in diamagnetism, fundamental WECE, Doppler-shifted WECE, and x-ray emissions. This indicates both density buildup and temperature buildup, with the former resulting from electron impact ionization of the neutral gas. Estimates based on Fig. 2(a) indicate achievement of heating rate "densities" on the order of 1 W/cm^3.

Floating potentials were generally negligible on probes located outside the ECRH resonance locations, as shown in Fig. 2(g). Directly at the resonance positions (approximately $\pm$ 5 cm), however, potential "depressions" up to $-$ 15 V were measured on the axially moveable probe toward the latter half of regime A. As the probe was moved further outside the resonance locations, the depressions occurred later and had smaller magnitude, as is evident in Fig. 2(g).

The plasma buildup and heating effect is also clearly evident in the evolution of the WECE spectra during regime A [Figs. 4(a)–4(c)]. The most dominant feature is the strong increase in the emission power with time, particularly at frequencies near the heating frequency of 7.43 GHz. Several other features should also be noted. At an early stage [Fig. 4(a)], we note two effects. First, the plasma is apparently confined between $\pm$ 7.5 cm (locations of 8.0 GHz cyclotron resonance). Second, a "dip" in the spectrum is observed between 6.55 (midplane resonance) and 7.0 GHz. It is hypothesized that this dip is caused by "cold" electron self-absorption effects in the vicinity of the midplane.[12] At a later time, in Fig. 4(b), we see that the dip effect is no longer observed, and, for frequencies near the heating frequency, the emission power level has increased by nearly an order of magnitude. As will be discussed later, the cold-electron self-absorption effect is probably still present, but now combines with the hot-electron spectrum to cause a sharp, monotonic decrease in emission power from 7.2 to 6.0 GHz.

Finally, at $t = 150$ μsec [in Fig. 4(c)], we observe the highest emission levels obtained in our experiment, just prior to the commencement of regime B. Again, several features of this figure warrant special mention. First, it is highly unlikely that the electron distribution function generating this spectrum is a simple Maxwellian with empty loss cone. For a mirror with a midplane cyclotron frequency of 6.55 GHz, a mirror ratio of 2, and a simple loss-cone Maxwellian, we would expect the WECE spectrum to vary more slowly over the range of 6.0 to 10.0 GHz. Instead, we observe a spectrum with a sharp peak near the heating frequency, 7.43 GHz, with a $1/e$ bandwidth of approximately 300 MHz. A more probable distribution causing the observed WECE spectrum would be what has been called a "sloshing electron" distribution.[13,14] Second, although the peak effect and its associated width near the heating frequency is most likely caused by a convolution of local and global emission and dispersion, one can proceed with an "extreme case" assumption that it is a purely local effect and thereby obtain estimates for upper bounds on both perpendicular and parallel "temperatures." For example, consider the case where the $1/e$ half-width of the peak is less than approximately 150 MHz. Postulating that this is caused solely by local relativistic broadening, we obtain the upper bound that $kT_\perp$ is less than 12 keV.[15] Alternatively, we can postulate that this is essentially a local

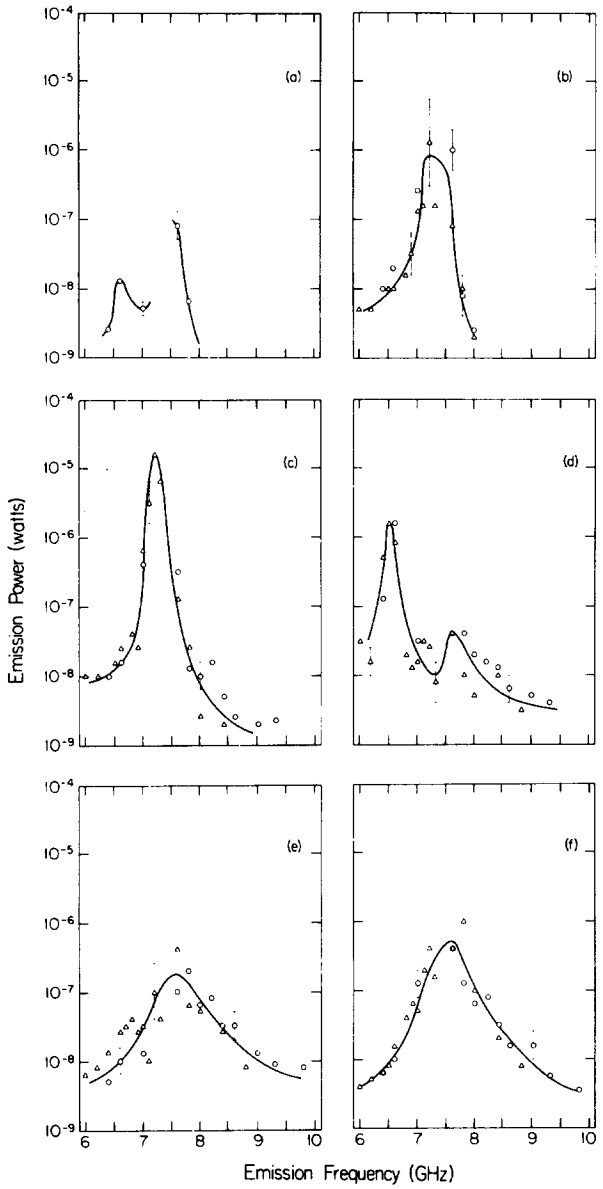

FIG. 4. Whistler emission spectra versus time from two separate runs. Circles represent data taken on 10/11/84, triangles for 12/1/84. Estimated errors include uncertainties caused by plasma fluctuations and frequency dependencies of the emission detection components. (a) 55 μsec, (b) 125 μsec, (c) 150 μsec, (d) 170 μsec, (e) 200 μsec, (f) 230 μsec.

Doppler-broadened effect which yields the upper bound that $kT_{\|}$ is less than 250 eV.[15]

The absence during regime A of a measurable electron density signal on the microwave interferometer [Fig. 3(e)] is a consequence of its axial position outboard of the ECRH resonance locations. Nevertheless, based on the presence of x-ray signals and the maximum temperature limits just established, it is reasonable to assume a perpendicular temperature $kT_{\perp}$ between 1 and 10 keV. Observed diamagnetism signals would then indicate electron densities during regime A between 1×10^{10} and 1×10^{11} cm^{-3}.

During the course of our experiments, we performed a series of runs in which we modulated the ECRH klystron so that the microwave power was turned off for 15 μsec and then restarted. Based on the results of these runs, we were able to estimate that the energy confinement time during regime A was greater than approximately 250 μsec. Furthermore, from the limits on plasma axial extent implied by the WECE spectra, we obtain an estimate for plasma volume of approximately 300 cm^3, assuming a plasma radius of 2.5 cm.

In another set of experiments we varied the ECRH power between discharges. One of the most important results presented in Fig. 5 was the scaling of heating rates with microwave power. The heating rates, or more accurately the heating rate densities (units of power per unit volume), were estimated from the instantaneous slopes of the integrated diamagnetic loop traces [for example, Fig. 2(a)]. The results of the different power levels were compared for equal perpendicular plasma pressure, $nkT_{\perp}$. This was done for two values of $nkT_{\perp}$: approximately 5×10^{13} and 10×10^{13} eV/cm^3, respectively. In both cases, the data fitted a scaling in which heating rate density varied as the square root of power.

One final observation regarding regime A should be discussed. By decreasing the vacuum base pressure and utilizing cw background gas feed, it was revealed that regime A's apparent stability was sensitive to the presence and species of background neutrals. Operation at the lowest achieved base pressures ($5–7\times10^{-7}$ Torr) using only puffed hydrogen (no cw feed) resulted in regime A demonstrating the same instability characteristics as regime B. A return to higher base pressure was achieved by controlled steady leakage of various gases (H_2, N_2) in combination with puffed hydrogen. Although stability of regime A was reestablished by this method, measurably higher base pressures were required when using hydrogen for the background gas as compared to nitrogen. Since the introduction of this background gas did not significantly reduce the diamagnetic loop signal, it was considered unlikely that the stabilization was a result of decreasing the hot-electron distribution anisotropy by increased electron–neutral collisions. Comparison of the hydrogen and nitrogen results, however, suggested the hypothesis that stabilization was being achieved by indirectly varying the relative percentage of "cold" electrons by virtue of the greater ionization efficiency of nitrogen as compared to hydrogen.[16] Such a cold-electron stabilization effect would agree with observations on other experiments.[17]

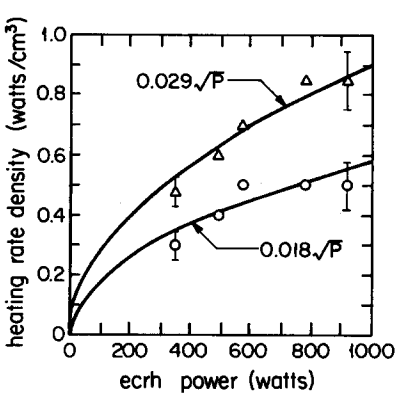

FIG. 5. Heating rate density versus ECRH power level. Triangles for $nkT_{\perp} = 10\times10^{13}$ eV/cm^3, circles for $nkT_{\perp} = 5\times10^{13}$ eV/cm^3.

B. Regime B

Regime B gives every indication of being micro-unstable with what we have tentatively identified as a whistler instability.[18,19] The most visible characteristic of this regime is the strong burst of microwave emission in the frequency range 6.4 to 6.6 GHz [Fig. 2(b)]. That this emission occurred at frequencies approximately less than or equal to any cyclotron fundamental frequency was confirmed by two methods. First, the magnetic field strength was increased until the heating frequency, 7.43 GHz, was resonant right on the midplane (further increase in the field resulted in the absence of resonant breakdown). Under these circumstances, the range of emission "burst" frequencies covered 7.2 to 7.4 GHz. Second, a measurement of the magnetic field confirmed that in the normal mode of operation, the midplane magnetic field strength corresponded to an electron-cyclotron frequency of approximately 6.55 GHz.

Other important characteristics of regime B include the coincident burst of enhanced electron endloss detected by both the NELD [Fig. 2(e)] and the microwave interferometer [Fig. 3(e)]. Because of the off-midplane position of the interferometer, this endloss burst is the first occurrence of measurable density at the interferometer's axial location. Measurements of the endloss burst on the NELD, however, indicated that approximately -20 V bias was sufficient to suppress this electron endloss signal. Additional negative bias, however, did not result in detectable ion endloss during the burst.

Another noticeable feature observed during regime B is the sudden decrease in the x-ray signal [Fig. 3(d)]. Although the other signals of regime B are quite reproducible, this sudden drop in x-ray signal is not. Thus, the reasons for its occurrence are not yet resolved and it remains a subject of continued study.

The implications of these measurements are summarized as follows. During regime B we observe a strong burst of whistler wave emission with a frequency below that of any fundamental cyclotron frequency in the mirror. Simultaneously, there is an occurrence of enhanced electron endlosses. The ejected electrons apparently have an average parallel energy within 20 V of the peak plasma potential inside the mirror. Thus, based on the temperature estimates for regime A, it is possible that these ejected electrons represented a highly anisotropic group, having a larger fraction of kinetic energy transverse to the magnetic field, rather than parallel.

During regime B, measurements of the floating potential inside the mirror reveal a rapid transition from zero or slightly negative values at the end of regime A (depending on axial location) to large positive values [Fig. 2(g)]. The axial variation of the potential at this time, presented in Fig. 6, shows a narrow, almost "square-well" profile between $z = \pm 10$ cm, with slight peaks near the resonance locations. This suggests that the electrons observed on the NELD most likely were trapped in this narrow midplane region prior to their escape.

Turning our attention to the WECE spectrum [Fig. 4(d)], we note several unique features during regime B. First, we observe the sharp peak in the frequency range where the

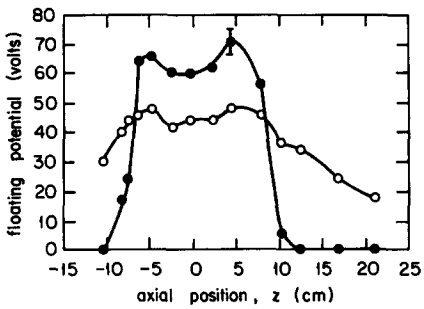

FIG. 6. Floating potential versus axial position for two different times. Blackened circles correspond to 170 μsec (during whistler instability), open circles to approximately 300 μsec (during MHD instability).

emission bursts are recorded (6.5 ± 1.0 GHz). Of equal interest, however, is the "hole" in the spectrum occurring approximately between the midplane frequency, 6.55 GHz, and the heating frequency, 7.43 GHz. Consideration of this spectrum, along with the other data discussed so far, suggests that these spectral features are a signature of a microinstability originating in the midplane region near the ECRH resonances. Emission near 6.5 GHz is enhanced by the instability [Fig. 2(b)]. The minimum near 7.4 GHz, however, is a consequence of diminished fundamental cyclotron emission caused by the rapid loss of electrons during the instability [Figs. 2(e), 3(d), and 3(e)].

Some additional information was obtained for this regime using the modulation experiments previously described. In this case it was possible to obtain both estimates for the energy confinement time and the plasma volume. These values were approximately 60 μsec and 750 cm^3, respectively. We note that the confinement time decreased from that of regime A, whereas the volume increased. Both of these characteristics indicate a microinstability that seeks to reduce the anisotropy of the electron distribution resulting from the ECRH during regime A.

Data presented in Fig. 7 from the ECRH power scan experiments illustrate that the amount of microwave energy "dumped" by the electron population via emission during

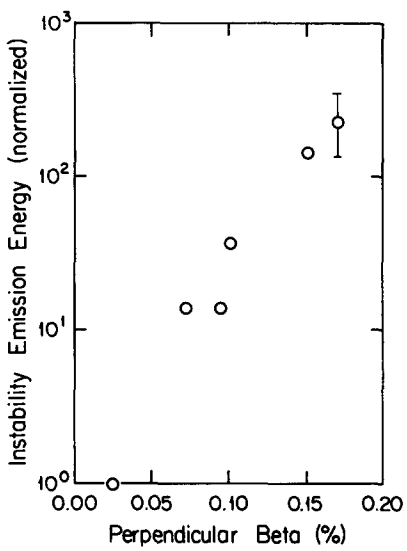

FIG. 7. Instability emission energy "dumped" by the plasma (6.5 GHz) during whistler instability versus perpendicular beta at the time of instability.

regime B increased with increasing $\beta_\perp = nkT_\perp/(B^2/8\pi)$. This is consistent with a whistler instability in which the transfer of electron perpendicular energy to instability wave energy results from a natural tendency of the electron distribution to isotropize.[20] The previously mentioned discovery that the instability-enhanced endloss involved low parallel-energy electrons is also in agreement with the results found in Ref. 20.

The previous data support the hypothesis that regime B is characterized by a microinstability resulting from the anisotropy of the electron velocity distribution function. The specific type of instability must now be confirmed. Our first observation is that for the ECRH power levels used in our experiments, the plasma pressure [see Fig. 2(a)] is too large for the instability to be a parametric mode.[21] The two most likely candidates, therefore, that would be consistent with microwave emissions at frequencies just below the electron-cyclotron frequency, are the whistler and the cyclotron maser instabilities. Furthermore, it is important to note that because of the relatively small scale lengths of these experiments, it is most probable that the instability involves an absolute rather than convective mode. It was previously mentioned that when the minimum (midplane) electron-cyclotron frequency in the mirror was 7.43 GHz, the instability-enhanced emission occurred over the range 7.2 to 7.43 GHz. Alternatively, when the minimum cyclotron frequency was set at 6.55 GHz, the instability emission covered 6.4 to 6.6 GHz. For identification purposes, discussion is focused on the lower end of these instability frequency ranges, 7.2 and 6.4 GHz, respectively.

Characterization of the whistler and cyclotron maser instabilities is often associated with the ratio of the real part of the instability frequency, f_R, to the local electron-cyclotron frequency f_{ce} where the instability originated.[18,22] For the minimum instability frequencies in our experiments, 7.2 and 6.4 GHz, the maximum value that such a ratio could have would involve the minimum cyclotron frequency in the mirror, i.e., 7.43 and 6.55 GHz, respectively. Thus, we have

$$(f_R/f_{ce}) \leqslant 7.2/7.43 \leqslant 6.4/6.55 < 0.98. \quad (1)$$

From the upper limit on $kT_\perp$ during regime A established from the WECE spectrum, however, the cyclotron maser instability should obey the relation[22]

$$0.99 \lesssim (f_R/f_{ce}) \lesssim 1.0 \quad (2)$$

for $kT_\perp$ less than 30 keV. In our experiments, we are able to resolve frequency and magnetic field measurements to three significant digits. Thus, the difference between our experimentally determined ratios, f_R/f_{ce}, and that expected for the cyclotron maser instability is significant.

In addition, studies have shown[23] that for $kT_\perp$ less than approximately 15 keV, absolute instability growth rates for the cyclotron maser instability are negligible. This is a natural consequence of the fact that azimuthal electron bunching which drives the cyclotron maser instability requires relativistic electron energies. In contrast, other investigations have shown[7,1819] that no such lower bounds on $kT_\perp$ exist for the absolute whistler instability, provided there is sufficient electron thermal anisotropy. For sloshing electron distributions, Guest and Sigmar[24] recognized that the regions near the ECRH resonance would be specifically susceptible to whistler instabilities caused by local high-energy anisotropies occurring in the regions of maximum density. Again, this is consistent with our WECE spectrum of Fig. 4(d), which suggests that the instability originates near the resonance zones. An important consequence of this is that Eq. (1) is more accurately expressed as

$$(f_R/f_{ce}) \leqslant 6.5/7.43 < 0.88. \quad (3)$$

From Ref. 18, a local thermal anisotropy of

$$T_\perp/T_z > 8$$

is sufficient to cause an absolute whistler instability characterized by Eq. (3). On the other hand, a cyclotron maser instability characterized by Eq. (3) would require electron temperatures in excess of 50 keV.[23] Such temperatures are inconsistent with the data of Figs. 2–4. Hence, regime B is most likely dominated by the whistler instability.

C. Regime C

The most visible characteristics of this regime are the presence of fluctuations (approximately 20 to 100 kHz) on many signals [see Figs. 2(d), 2(f), and 2(g)] and the marked decrease in diamagnetism [Fig. 2(a)]. The WECE signals of Figs. 2(b) and 2(c) during regime C exhibited a slow decrease towards levels characteristic of the "thermal" emissions of regime A. This decrease is less apparent than the diamagnetism change since the emission signals are on a logarithmic scale, whereas the diamagnetism is measured on a linear scale. Endloss currents at this time were significant, and included both ion and electron flux [Figs. 2(d) and 2(f)]. Furthermore, estimates of energy confinement times obtained from the previously mentioned modulation experiments indicated that this regime had the lowest values: approximately 10 to 30 μsec. Plasma volume estimates from the same experiments indicated an increase from regime B to approximately 1200 cm^3. Finally, the interferometer signal [Fig. 3(e)], the WECE spectra [Figs. 4(e) and 4(f)], and the axial potential profile (Fig. 6) illustrate the observed axial plasma expansion during this regime as compared to regimes A and B.

The above observations along with the large quantity of others' experience with axisymmetric mirrors[25] led to the hypothesis that the behavior of this regime in our experiment was dominated by flute-like MHD instabilities. Futher evidence for this hypothesis was obtained when we positioned two electrostatic probes at a common axial location but different azimuthal positions. Comparison of the floating potential traces from these two probes revealed a phase relationship that was consistent with $m = 1$ gravitational flute modes resulting from the magnetic field curvature [Fig. 2(g)].

It should be noted that the probe signals of Fig. 2(g) end at an earlier time than the signals of Figs. 2(a)–2(f). This result was caused by a shorter microwave pulse for the data of Fig. 2(g) as compared to that in Figs. 2(a)–2(f) and Fig. 3.

An unanticipated benefit resulted from the occurrence of regime C. Because of the axial location of the microwave interferometer, it was not possible to measure electron densi-

ties with this diagnostic during regime A. The isotropization and consequent plasma axial expansion caused by the MHD instability, however, did permit a measurement of radially averaged plasma density after 200 μsec. Although this density measurement was subsequent to regime B, it was considered to be a useful order-of-magnitude estimate for the peak density achieved from the buildup during regimes A and B. For an estimated plasma diameter of 5 cm, Fig. 3(e) indicates a peak density of approximately 2.3×10^{12} cm^{-3}. In spite of the fact that such a density implies a plasma frequency above cutoff for 7.43 GHz radiation, the reflected power of Fig. 3(c) was observed to decrease during regime C. While a detailed study of the reasons for this decrease has not been pursued, the mere fact that reflection did not increase as densities approached the critical density was considered to be a good demonstration of the efficacy of whistler mode ECRH for high-density plasmas.[5]

The initial buildup phase appears well-characterized by separate groups of cold and hot electrons. Therefore, during regime A the diamagnetism and WECE signals are likely dominated by hot-electron contributions. After the whistler and MHD instabilities of regimes B and C, however, the electrons have been mixed and isotropized resulting in a single group of "warm" electrons. Thus, after 200 μsec the diamagnetism drops by nearly a factor of 4 because of the effective reduction of electron energy. This effect is also seen in the WECE signals of Figs. 2(b) and 2(c), which show a decrease of almost 6 dB between 150 and 400 μsec.

IV. THEORETICAL MODELING

In order to understand the results of regime A, we have simulated the evolution of an electron velocity distribution function under the influence of whistler mode ECRH. This work has been performed using a quasilinear, Fokker–Planck computer code developed at the Lawrence Livermore National Laboratory.[26] Initial results presented in Fig. 8 gave a clear indication that the electron velocity distribution becomes strongly anisotropic at a very early stage, in agreement with recent results reported by Mauel.[27]

We have compared our measured WECE data to that predicted by a computer model developed by Tsakiris and Ellis.[10] The unique peaked nature of our spectra, however, prompted special attention to the selection of model axial profiles for electron densities and temperatures. Having written a numerical subroutine that self-consistently calculated axial profiles by assuming a midplane velocity distribution and conserving magnetic moment, we considered the proper choice of midplane distribution. Based on the results of our Fokker–Planck simulations in Fig. 8, we choose to consider a hot anisotropic electron distribution of the form

$$f(\mathbf{v}) = \eta \exp(-v^2/\alpha^2) g(\theta), \tag{4}$$

where η is a normalization coefficient, α is a "thermal" speed, and $g(\theta)$ is so far an unspecified function of midplane velocity pitch angle. In particular, as seen in Fig. 9 the data support the choice of the hot-electron, model-pitch-angle distribution

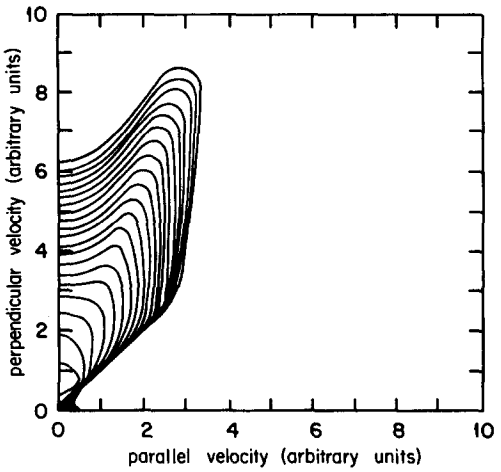

FIG. 8. Example of velocity space contour plot for electron velocity distribution after ECRH as predicted by Fokker–Planck numerical simulations.

$$g(\theta) = \begin{cases} \exp\{-[(\theta-\theta_R)/\psi_1]^2\}, & \sin\theta_R \leqslant \sin\theta \leqslant 1, \\ \exp\{-[(\theta-\theta_R)/\psi_2]^2\}, & \sin\theta_{lc} \leqslant \sin\theta \leqslant \theta_R, \\ 0; & 0 \leqslant \sin\theta < \sin\theta_{lc}, \end{cases} \tag{5}$$

where θ_{lc} is the loss-cone angle, θ_R is the midplane pitch angle for electrons with mirror turning points at the ECRH resonance locations, and ψ_1 and ψ_2 are empirically adjusted parameters. The ability of this model distribution to approximate the results of the Fokker–Planck calculations is demonstrated in Fig. 9(a), which is to be compared to Fig. 8. Also, as seen in Fig. 9(b), this distribution is associated with peaks in hot-electron density at the ECRH resonance locations, a feature also reported in similar experimental studies.[14] In agreement with observations reported previously in this article, as well as results reported by other investigators,[13,28] these hot density peaks tend to generate local potential depressions. For the experiments discussed here, such depressions reached approximately -15 V at the resonances. These potentials are sufficient to confine a Maxwellian cold-electron population (cold electrons resulting from ionization) with a temperature of approximately 10 eV or less by virtue of the Boltzmann factor $\exp[-\Phi(z)/T_c]$. We have simulated this anticipated cold population as a second electron component with an axial density profile $n_c(Z=0)\exp[-(z/L_c)^2]$ and an axially constant temperature. Figure 9(c) demonstrates that inclusion of the midplane-confined cold electrons is important to obtain improved agreement between the experimentally observed and the theoretically predicted spectra. The presence of a cold-electron component is also consistent with the observations regarding the stability of regime A to the whistler instability.

Comparison has also been made between our experimental heating rate densities with those predicted by theory. A number of authors have recently modeled ECRH as an rf-induced velocity space diffusion. In particular, we have chosen to compare our results with the predictions of two such models.[29,30]

In the first instance, the conditions of our experiment closely resemble the parameters used to obtain Fig. 2 of Ref. 29. If we postulate a simplistic electron energy distribution

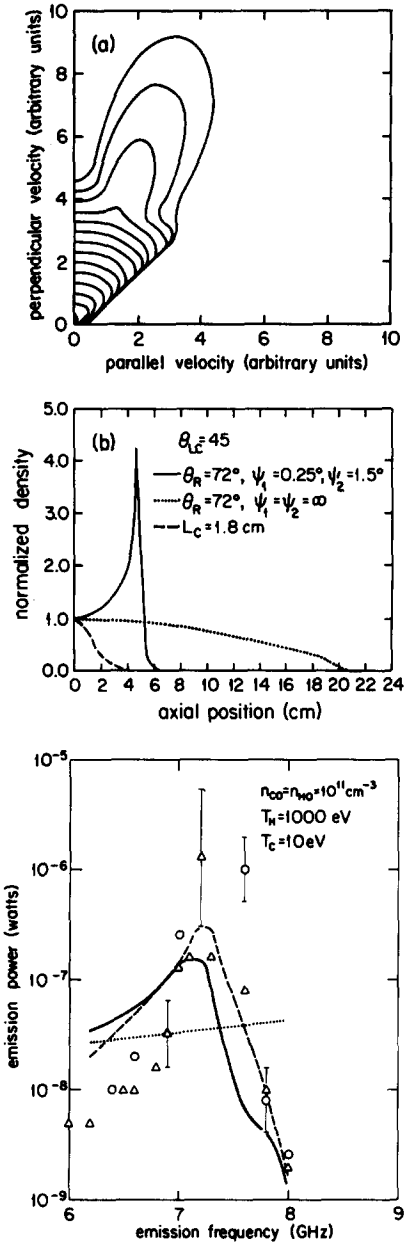

FIG. 9. Theoretical analysis of WECE during regime A. (a) velocity space contour plot for a combination of a cold, loss-cone Maxwellian and the assumed hot, sloshing-electron distribution of Eq. (5); (b) model electron density axial profiles for hot sloshing (solid) and hot, loss-cone Maxwellian distributions (dotted), and midplane-confined cold electrons (dashed); (c) comparison of the observed whistler emission spectrum at 125 μsec with theoretical predictions for various electron distributions. Dotted line is for hot loss-cone Maxwellian; solid line is for hot sloshing electrons alone; dashed line is for hot sloshing and cold midplane-trapped electrons combined. Theoretical spectra have been normalized so that $P(7.2\ \text{GHz}) = 3\times10^{-7}$ W for the dashed line case.

function (taken at the midplane) of the form

$$f(w_\parallel, w_\perp) = F(w_\parallel)\delta(w_\perp - T_{\perp_0}) \tag{6}$$

(where $w_\parallel$, $w_\perp$ are the electron parallel and perpendicular energies, respectively) and we assume a perpendicular "temperature" $T_{\perp_0}$ of 1000 eV [a very feasible choice, considering Fig. 2(a)] then the model of Ref. 29 would suggest a per-particle heating rate of 0.8 to 1.6×10^{-10} W. Multiplying this by an electron density of approximately 10^{10} cm^{-3} [also consistent with Fig. 2(a) for $T_{\perp_0} \simeq 1000$ eV] yields the theoretical heating rate density prediction of approximately 1 W cm^{-3}, in good agreement with our experimentally measured rates.

From the results of the second model,[30] one can obtain an expression for the gain in perpendicular energy of a single electron passing through resonance,

$$\Delta w_\perp \simeq (1/2m)\{[eE\tau_{\text{eff}}]^2 + 2meE\tau_{\text{eff}} v_{\perp,\text{res}} \cos(\varphi)\} \tag{7}$$

or

$$\Delta w_\perp \simeq \Delta w_d + \Delta w_s\ , \tag{8}$$

where we define

$$\Delta w_d = (1/2m)[eE\tau_{\text{eff}}]^2,$$
$$\Delta w_s = eE\tau_{\text{eff}} v_{\perp,\text{res}} \cos(\varphi). \tag{9}$$

Here, m is the electron mass, e the electron charge, E the ECRH electric field strength, τ_{eff} the effective time the electron remains in resonance with the electric field, $v_{\perp,\text{res}}$ the electron perpendicular velocity as it reaches the resonance position, and φ is related to the change in the electron's gyrophase as it passes through resonance. The first term on the right-hand side of Eq. (8), Δw_d, represents the deterministic acceleration of the electron in the presence of the electric field

$$\frac{dv}{dt} = \frac{eE}{m}\ . \tag{10}$$

The second term Δw_s represents a stochastic heating effect[30] for our experimental parameters. With this information a heating rate could be calculated by computing a second velocity moment of the bounce-averaged velocity space transport equation

$$\frac{\partial f}{\partial t} = -\frac{\partial}{\partial \mathbf{v}} \cdot \Gamma_v \tag{11}$$

to obtain

$$\frac{\partial nT}{\partial t} = -\int d^3v \left(\frac{\partial}{\partial \mathbf{v}} \cdot \Gamma_v\right)\left(\frac{1}{2} mv^2\right). \tag{12}$$

In these equations, Γ_v represents an rf-induced velocity space "current" of the form

$$\Gamma_v = \left\langle \frac{\Delta \mathbf{v}}{\Delta t} \right\rangle f(\mathbf{v}) + D_v \frac{\partial f(\mathbf{v})}{\partial \mathbf{v}}\ . \tag{13}$$

Here, $\langle \Delta \mathbf{v}/\Delta t \rangle$ is a "drag" coefficient and D_v is a velocity diffusion coefficient derived from the deterministic and stochastic terms of Eq. (8), respectively. These velocity space transport coefficients are calculated with the help of the following approximate formulas:

$$\left\langle \frac{\Delta \mathbf{v}}{\Delta t} \right\rangle \simeq \left\langle \frac{1}{mv_\perp} \frac{\Delta w_\perp}{\Delta t} \right\rangle_\varphi \simeq \frac{1}{mv_\perp} \frac{\Delta w_d}{\tau_B/2}\ ,$$
$$D_v \simeq \left\langle \frac{\Delta v_{\perp,s}^2}{\Delta t} \right\rangle \simeq \frac{(2/m)\langle \Delta w_s \rangle_{\text{rms}}}{\tau_B/2}\ , \tag{14}$$

where τ_B is the electron mirror bounce period. The following assumptions are now employed. First, we neglect the electrostatic potential in order to simplify computation of a heating rate estimate. Also, the data suggest that negligible

potentials form within the mirror during regime A. Second, we assume that only electrons that have mirror turning points, z_T, which lie beyond the resonance location, z_{res}, experience energy gain from the ECRH. Thus, we use the form[30] for τ_{eff}

$$\tau_{eff} \simeq 2(\pi \lambda v_{\parallel,res} \omega_s/2)^{-1/2}, \quad \lambda \simeq \frac{1}{B}\frac{dB}{dz}\bigg|_{z=z_{res}}. \tag{15}$$

Third, we estimate an electric field strength E based on a plane wave model in which the ECRH energy is homogeneously distributed over the cross-sectional area of the vacuum vessel. Finally, we must assume a form for the distribution function $f(\mathbf{v})$. Again, based on the results from the numerical simulations (Fig. 8), we employ the distribution function of Eqs. (4) and (5). Combining Eqs. (8) and (9), and (12)–(15), and assuming values for ψ_1, ψ_2, θ_{lc}, and θ_R of Eq. (5) of 20°, 10°, 45°, and 70°, respectively, we perform some numerical integrations to finally obtain

$$\dot{W} \equiv \frac{\partial nT}{\partial t} \simeq (4.9\times 10^{-15}) Pn + (1.9\times 10^{-14})\sqrt{P}\, nT^{3/4} \tag{16}$$

in W/cm^3 provided that the density n is in units of cm^{-3} and the ECRH power P is units of W. The first term of Eq. (16) occurs because of the deterministic heating and the second results from the rf diffusion. The "temperature," $T \simeq (m\alpha^2)/2e$, is in units of eV. First, we note that the stochastic heating term dominates the deterministic term if

$$T > 0.2(P)^{2/3}. \tag{17}$$

This will be satisfied for ECRH powers of 900 W or less, provided that T is greater than approximately 20 eV. For the levels of diamagnetism achieved in our experiments, such a condition is almost certainly satisfied. When Eq. (17) is satisfied, Eq. (16) approximately reduces to

$$\dot{W} \simeq (1.9\times 10^{-14})\sqrt{P}\, nT^{3/4}. \tag{18}$$

Second, if we acknowledge that holding $nT_\perp$ constant is approximately equivalent to holding $nT^{3/4}$ constant, then the data presented in Fig. 5 are in good agreement with Eq. (18) for the scaling of heating rate density with ECRH power P. Third, the data of Fig. 5 were obtained for two different values of $nT_\perp$, 5×10^{13} and 10^{13} eV/cm^3, respectively. If we assume that these two values of $nT_\perp$ were the result of a doubling in "temperature" $T_\perp$ while density remained approximately constant, then Eq. (18) predicts that the heating rate densities for the two levels of $nT_\perp$ should obey the relationship

$$\dot{W}_2/\dot{W}_1 \simeq (nT_{\perp 2}/nT_{\perp 1})^{3/4} \tag{19}$$

for constant power P. From Fig. 5 it is determined that for $nT_\perp = 5\times 10^{13}$ and $nT_{\perp 2} = 10\times 10^{13}$,

$$\dot{W}_2/\dot{W}_1 \simeq 0.029/0.018 \simeq 1.61, \tag{20}$$

whereas

$$(nT_{\perp 2}/nT_{\perp 1})^{3/4} \simeq (10/5)^{3/4} \simeq 1.68, \tag{21}$$

again demonstrating good agreement between the simplified model of Eq. (18) and the experimental results. Finally, if the electron density, temperature, and ECRH power are again assumed to be approximately 10^{10} cm^{-3}, 1000 eV, and 900 W, respectively, one obtains an estimated heating rate density of approximately 1 W cm^{-3}, again in good agreement with typical experimental values.

V. SUMMARY AND CONCLUSIONS

We have presented experimental results on ECRH startup and heating using the whistler mode in an axisymmetric mirror. Both the data and numerical simulations indicate the rapid creation of a strongly anisotropic electron velocity distribution, possibly achieving a "sloshing-electron" form. This results in a whistler instability, which is accompanied by enhanced electron endlosses and strong bursts of microwave emission at frequencies slightly below the fundamental electron-cyclotron frequency. It was found that the onset of this instability is sensitive to the presence of background neutrals, probably because of a cold electron stabilization effect. Eventually, MHD instabilities occur, reducing both particle and energy confinement and causing axial plasma expansion.

Electron densities were achieved during startup which exceeded the critical density for the 7.43 GHz heating frequency. Nevertheless, reflected power decreased instead of increasing. This is consistent with the absence of a cutoff density for ECRH startup using the whistler mode.

It has been demonstrated that the time-resolved whistler mode electron-cyclotron emission spectrum is a particularly valuable diagnostic for studying ECRH startup and heating in mirrors by providing information on plasma axial extent, electron velocity distribution anisotropy, and the axial location(s) where microinstabilities originate. A strongly anisotropic electron distribution function model needed to match observed emission spectra and predictions of a computer model agreed with the results of numerical Fokker–Planck simulations.

Finally, simplified theoretical analysis using existing models for stochastic ECRH provides predictions for heating rates that are in good agreement with experimental results.

ACKNOWLEDGMENTS

We thank Professor R. F. Ellis and C. Lasnier of the University of Maryland and Dr. R. James of the Lawrence Livermore National Laboratory for important discussions on whistler mode cyclotron emission. Tim Goodman, Eric Pitcher, and Dave Whaley provided valuable experimental assistance.

This research as partially supported by the National Science Foundation. The first author (J. H. B.) gratefully acknowledges the support of a U. S. Department of Energy Magnetic Fusion Energy Technology Fellowship. The authors also thank the Lawrence Livermore National Laboratory for contributing the computer time to perform the Fokker–Planck analysis. In addition, we wish to thank the Environmental Research Institute of Michigan for generously loaning the broadband oscillator used in the cyclotron emission heterodyne detection circuit.

[1]R. Breun, S. N. Golovato, L. Yujiri, B. McVey, A. Molvik, D. Smatlak, R. S. Post, D. K. Smith, and N. Hershkowitz, Phys. Rev. Lett. **47**, 1833 (1981).
[2]D. E. Baldwin and B. G. Logan, Phys. Rev. Lett. **43**, 1318 (1979).
[3]D. P. Grubb, S. A. Allen, T. A. Casper, J. F. Clauser, F. H. Coensgen, D. L. Correll, W. F. Cummins, C. C. Damm, J. H. Foote, R. K. Goodman, D. N. Hill, E. B. Hooper, Jr., R. S. Hornady, A. L. Hunt, R. G. Kerr, G. W. Leppelmeier, J. Marilleau, J. M. Moller, A. W. Molvik, W. E. Nexsen W. L. Pickles, G. D. Porter, P. Poulsen, E. H. Silver, T. C. Simonen, B. W. Stallard, W. C. Turner, W. L. Hsu, T. L. Yu, J. D. Barter, T. Christensen, G. Dimonte, T. W. Romesser, R. F. Ellis, R. A. James, C. J. Lasnier, L. U. Berzins, M. R. Carter, C. A. Clower, B. H. Failor, S. Falabella, M. Flammer, and T. Nash, Phys. Rev. Lett. **53**, 783 (1984).
[4]B. W. Stallard, IEEE Trans. Plasma Sci. **12**, 134 (1984).
[5]N. T. Lam, J. E. Scharer, and K. R. Audenaerde, IEEE Trans. Plasma Sci. **13**, 25 (1985).
[6]D. Sing, S. N. Golovato, N. Hershkowitz, and J. Scharer, Phys. Fluids **27**, 16 (1984).
[7]S. J. Gitomer and J. L. Shohet, Phys. Fluids **13**, 413 (1970).
[8]Y. Matsuda (private communication).
[9]R. F. Ellis, G. D. Tsakiris, and D. A. Boyd, Phys. Rev. Lett. **48**, 93 (1982).
[10]G. D. Tsakiris and R. F. Ellis, Nucl. Fusion **23**, 1115 (1983).
[11]R. F. Ellis (private communication).
[12]R. F. Ellis, R. A. James, C. J. Lasnier, and T. A. Casper, Rev. Sci. Instrum. **56**, 891 (1985).
[13]J. Kesner, Nucl. Fusion **21**, 97 (1981).
[14]G. R. Haste and N. H. Lazar, Phys. Fluids **16**, 683 (1973).
[15]G. Bekefi, *Radiation Processes in Plasmas* (Wiley, New York, 1966), pp. 184–202.
[16]J. T. Tate and P. T. Smith, Phys. Rev. **39**, 270 (1932).
[17]T. A. Casper (private communication).
[18]J. E. Scharer and A. W. Trivelpiece, Phys. Fluids **10**, 591 (1967).
[19]L. S. Hall and J. E. Scharer Phys. Fluids **16**, 2352 (1973).
[20]S. L. Ossakow, I. Haber, and E. Ott, Phys. Fluids **15**, 1538 (1972).
[21]M. Porkolab and R. P. H. Chang, Rev. Mod. Phys. **50**, 745 (1978).
[22]P. L. Pritchett, Phys. Fluids **27**, 2393 (1984).
[23]Y. Y. Lau and K. R. Chu, Phys. Rev. Lett. **50**, 243 (1983).
[24]G. E. Guest and D. J. Sigmar, Nucl. Fusion **11**, 151 (1971).
[25]M. S. Ioffe and R. I. Sobolev, Plasma Phys. J. Nucl. Energy, Part C7, 501 (1965); C. W. Hartman, Phys. Fluids **10**, 1685 (1967).
[26]Y. Matsuda and J. J. Stewart, *Proceedings of the Tenth Conference on Numerical Simulation of Plasmas*, San Diego, CA, 4–6 January 1983 (G. A. Technologies, Inc., San Diego, CA, 1983), p. 2B8.
[27]M. E. Mauel, Phys. Fluids **27**, 2899 (1984).
[28]P. K. Smith, Ph. D. thesis, University of Wisconsin, 1983.
[29]P. K. Smith, Plasma Phys. Controlled Fusion **26**, 461 (1984).
[30]P. Jaeger, A. J. Lichtenberg, and M. A. Lieberman, Plasma Phys. **14**, 1073 (1972); M. A. Lieberman and A. J. Lichtenberg, Plasma Phys. **15**, 125 (1973).